Materials Reports
Solidwaste & Ecomaterials

Materials Reports: Solidwaste and Ecomaterials

Journal Homepage: www.sciopen.com/journal/3078-4093

Original Research Report

Co-utilization of sewage sludge and brine sludge for the preparation of porous ceramsite: Properties, phase transformation, and heavy metal immobilization

Gelong Xu [1, 2], Jiaqi Zhang [1, 2], Jiwei Cai [1, 2], Feiyu Wang [3], Yang Liu [3], Xinyuan Feng [4], Yaguang Wang [2], Zixuan Du [4], Qing Tian [1, 2, *]

[1] Kaifeng Research Center for Engineering Repair and Material Recycle, Henan University, Kaifeng 475004, China

[2] School of Civil Engineering and Architecture, Henan University, Kaifeng 475001, China

[3] China Construction Eighth Engineering Division Co., LTD (North China), Tianjin 300450, China

[4] Miami College, Henan University, Kaifeng 475004, China

Abstract: The co-utilization of multi-source solid waste is a promising approach for sustainable industrial development. This study aims to incorporate Fe-rich sewage sludge, fly ash, and brine sludge into sintered ceramsite. With sewage sludge as the predominant constituent, the influence of fly ash and brine sludge as regulatory constituents on the mechanical and physical properties of the sintered ceramsite is investigated, and the mechanism is elucidated through a comprehensive analysis of phase transformation and microstructure. The ceramsite with 90% sewage sludge and 10% fly ash exhibits a particle compressive strength of 7.13 MPa and an apparent density of 1280 kg m^{-3}. The mineral composition of sintered ceramsite is mainly quartz, anorthite, hematite, and pyroxene. The addition of brine sludge promotes the melting of quartz and hematite, leading to increased pyroxene formation and enhanced compressive strength. Adding 15% brine sludge can convert almost all of the hematite into pyroxene, and the specific strength of ceramsite increases from 5.6 × 10^{-3} to 7.8 × 10^{-3} MPa m^3 kg^{-1}. Furthermore, the ceramsite made from sewage sludge, fly ash, and brine sludge exhibits a minimal risk of heavy metal leaching. The findings provide a reference for the performance optimization of sludge-based ceramsite.

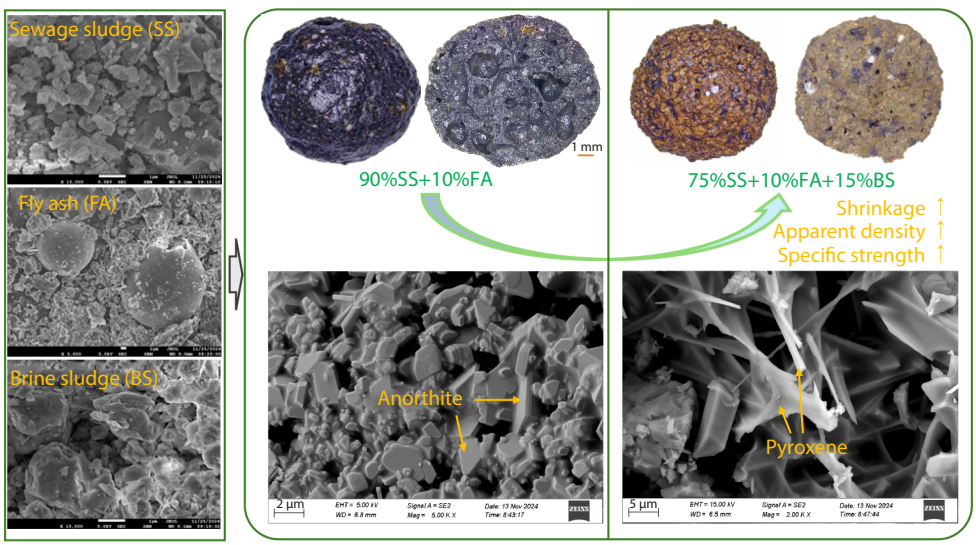

Keywords: ceramsite, sewage sludge, brine sludge, mechanical properties, phase transformation

Citation: G. Xu, J. Zhang, J. Cai, et al. Co-utilization of sewage sludge and brine sludge for the preparation of porous ceramsite: Properties, phase transformation, and heavy metal immobilization. *Materials Reports: Solidwaste and Ecomaterials*, 2026, 2: 9520027. https://doi.org/10.26599/MRSE.2026.9520027.

*Correspondence to Q. Tian, 10160090@vip.henu.edu.cn

Received 23 December 2025; Received in revised form 13 April 2026; Accepted 28 April 2026

1. Introduction

Sewage sludge is a solid waste generated during sewage treatment. According to the *China Urban Construction Statistical Yearbook 2022*, China's dry sewage sludge generation was 15.75 million tons in 2022, with a disposal rate of 99.31%[1]. However, prevailing disposal methods are conventional, i.e., landfill and incineration, which can adversely affect the environment and human health, and the overall utilization efficiency remains low[2,3]. In addition to its abundance of organic matter, sewage sludge also comprises inorganic constituents such as Al_2O_3, SiO_2, CaO, and Fe_2O_3, which are valuable for recycling in the production of construction materials[4,5]. It is thought that the production of lightweight sintered ceramsite is a promising approach to utilizing sewage sludge, with the pore-forming effect of organic matter in pyrolysis, and heavy metals can also be solidified during the sintering process to reduce pollution and environmental damage[6]. Moreover, the cost of ceramsite preparation is comparable to, and even lower than, that of shale ceramsite, fly ash ceramsite, and clay ceramsite[7].

The fabrication of lightweight porous ceramsite is a straightforward process that utilizes sewage sludge and the gasification of organic matter. In addition to adequate pore-forming ability, pore structures also need to be considered, as they significantly affect the properties of lightweight ceramsite and are related to phase transformations during sintering. It can be concluded that the sludge ceramsite belongs to the SiO_2-Al_2O_3-flux system[8]. The presence of SiO_2 and Al_2O_3 as the main skeleton components substantially influences liquid-phase viscosity, thereby impacting the efficacy of pore trapping[9]. Flux ingredients, including CaO, MgO, Na_2O, K_2O, and Fe_2O_3, affect the formation of pore structures by altering the eutectic point and the yield of liquid phase[8,10,11]. The ideal scenario is for the formed pores to be efficiently captured by the liquid phase during the melting of inorganic oxides, with these pores distributed evenly within the matrix. According to the Riley triangle theory, the appropriate ranges of SiO_2, Al_2O_3, and flux are 53%–79%, 10%–25%, and 13%–26%, respectively. However, this ingredient is not feasible to prepare sludge ceramsite. Tsai et al.[8] claimed that in consideration of the bloating performance, the suitable ratios of SiO_2, Al_2O_3, and flux were 35%–44%, 10%–26%, and 36%–44% for sewage sludge ceramsite, respectively. Xu et al.[12] found that Al_2O_3 contents between 18% and 26% and SiO_2 between 30% and 45% were beneficial for the strength of wastewater ceramsite with densified surfaces. For sewage sludge with unsatisfactory inorganic components, supplementary materials, such as clay, fly ash, waste glass powder, river sediment, blast furnace slag, and red mud, are generally used to regulate the skeleton and flux components, thereby improving the quality of ceramsites[5,8,9,13–15]. The concurrent utilization of multiple solid waste sources is gaining popularity to optimize ceramsite production efficiency.

High strength is generally contradictory to the porous structure of ceramsite. However, a relative balance between high strength and light weight can be achieved by optimizing the phase constituents, thereby enhancing the matrix in the sintered ceramsite. The matrix consists of a vitreous binder with embedded crystalline phases, and the typical crystalline phases include Na–Ca feldspar, hematite, and mullite[16–18]. Anorthite is a particularly promising phase in ceramsite, with the potential to yield superior performance[16,19,20]. In addition, it has been demonstrated that diopside, as a target phase, contributes significantly to the strength of lightweight ceramsite[21]. With the presence of Fe_2O_3, complex crystalline phases with greater diversity form[22]. Some studies[23,24] reported that the transformation of Fe_2O_3 into pyroxene or diopside improves the mechanical properties of ceramsite. This provides an idea for the high-strength ceramsite from Fe-rich raw materials. However, in this case, it should be noted that appropriate regulation of CaO content is necessary to maintain electrical neutrality within silicate networks for phase formation[22].

Brine sludge is an industrial waste material from the chlor-alkali industry. In China, the annual output of brine sludge is approximately 3.5 million tons[25]. Due to the presence of harmful or toxic substances, such as heavy metals, landfill disposal requires large areas of land and causes soil, water, and air pollution[26–28]. Hence, it is important to explore safe approaches to brine sludge recycling. The chemical composition of brine sludge is typically dominated by $CaCO_3$, with smaller amounts of $Mg(OH)_2$ and NaCl[29,30]. Brine sludge can be used as a raw material for cement production, a desulfurization agent in thermal power plants, an adsorbent for sewage treatment, and a filler for artificial stone, rubber, and paper production[30]. Despite its extensive range of applications, these uses frequently necessitate complex pretreatment processes, which limit the comprehensive utilization of brine sludge due to technical and cost constraints. For instance, brine sludge can be used on a large scale as an alternative raw material to limestone in cement production. However, to eliminate the adverse effects of chlorine, the brine sludge must be purified, which in turn increases investment in technology and equipment. As reported by previous studies[13,14,31], $CaCO_3$ can be used as a pore-forming agent and calcium source in the fabrication of porous sintered ceramsite. Therefore, from a chemical composition perspective, it is feasible to use brine sludge to produce sintered ceramsite, but relevant research remains very limited.

This study utilizes Fe-rich sewage sludge as the main raw material to prepare sintered ceramsite. By incorporating fly ash and brine sludge, pyroxene is considered the target phase to enhance the strength of sintered ceramsite. Fly ash is used to adjust the initial SiO_2 and Al_2O_3 content of ceramsite. On this basis, the study focuses on the effects of the replacement ratio of brine sludge for sewage sludge on the physical and mechanical properties, phase transformation, and microstructure of sintered ceramsite. The findings are expected to serve as a reference for the co-utilization of solid wastes and the preparation of high-strength ceramsite.

2. Materials and methods

2.1. Materials

The raw materials employed in this study included sewage

sludge (SS), brine sludge (BS), and fly ash (FA), all of which were collected from Kaifeng, China. The chunky sewage sludge and brine sludge were ground in a ball mill for 3 h to obtain a powder with particle sizes below 75 μm. The chemical compositions of the raw materials are listed in Table 1, and their particle size distributions are shown in Fig. 1. SS has a high content of Fe_2O_3. FA has higher SiO_2 and Al_2O_3 contents than SS, and BS is rich in CaO. The minerals in the raw materials were determined by XRD analysis, as illustrated in Fig. 2. The mineralogical analysis revealed that SS and FA had similar mineral compositions, including quartz, calcite, and albite. Notably, the presence of hematite in FA was characterized by its strong diffraction intensity. Furthermore, the XRD analysis revealed that the chemical composition of BS is $CaCO_3$, existing in two crystalline forms: calcite and aragonite. The SEM images of the raw materials are also provided in Fig. 2, illustrating the presence of microbeads in FA and the observation of a hollow structure in some of them.

Table 1. Chemical compositions of raw materials.

Chemical composition	SS (%)	FA (%)	BS (%)
SiO_2	33.91	44.47	1.67
Fe_2O_3	18.05	10.26	0.29
CaO	17.17	9.89	86.69
Al_2O_3	12.70	26.70	0.39
SO_3	4.82	2.73	0.45
P_2O_5	4.55	0.21	—
MgO	3.80	1.70	4.80
K_2O	1.66	1.32	0.17
TiO_2	1.12	1.20	—
CuO	0.57	—	—
ZnO	0.39	—	—
MnO	0.35	0.10	—
Cl	0.20	—	3.69
SrO	0.12	0.07	1.73
Cr_2O_3	0.08	—	—
Na_2O	—	1.10	—
Other	0.49	0.23	0.08

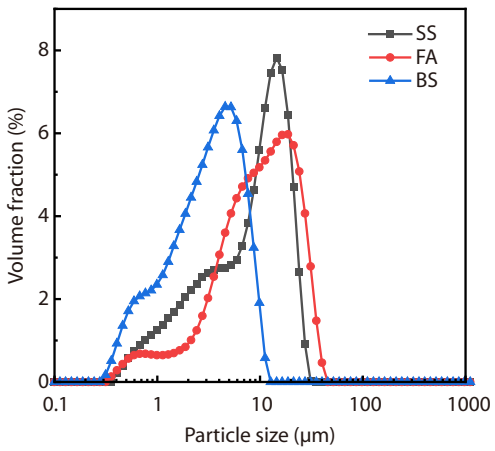

Fig. 1. Particle size distributions of raw materials.

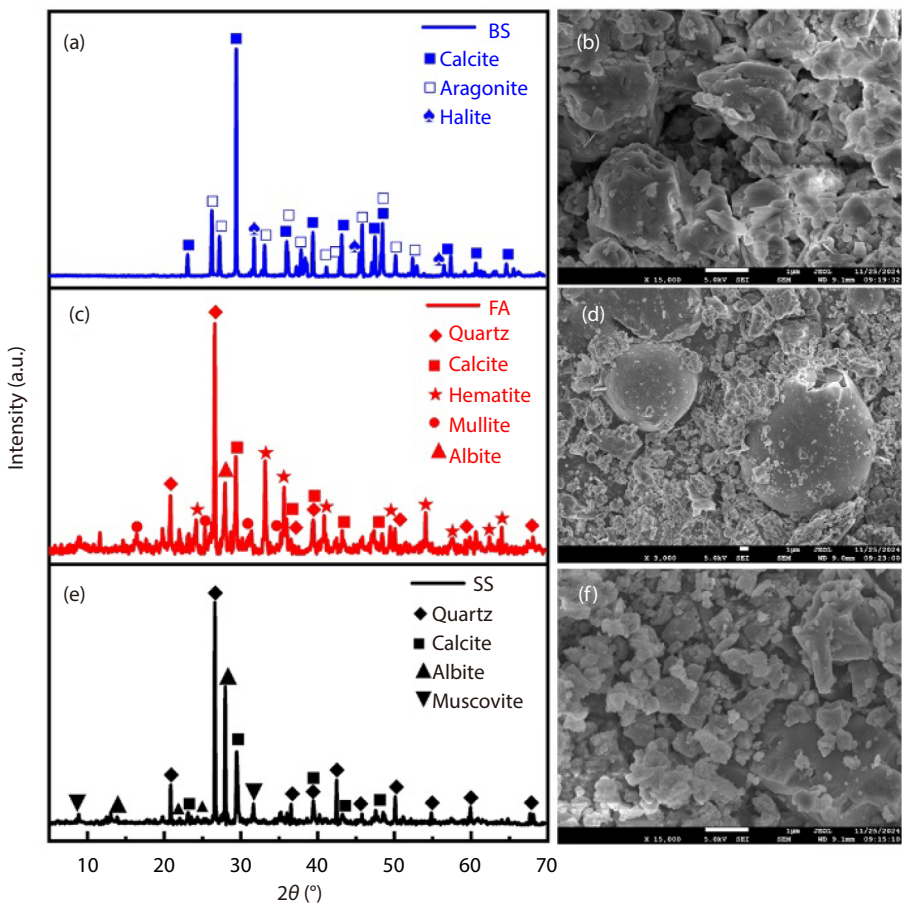

Fig. 2. XRD patterns and SEM images of raw materials: (a, b) BS, (c, d) FA, and (e, f) SS.

2.2. Preparation of sintered ceramsite

As detailed in Table 2, two series of the material constituents of ceramsite were designed. After deducting the mass loss caused by pyrolysis determined from the TG results of raw materials, the chemical composition of the designed ceramsites is calculated based on the XRF results and is also listed in Table 2. C1, C2, and C3 ceramsites contain 20%, 15%, and 10% FA, respectively. The partial replacement of SS with FA increases the SiO_2 and Al_2O_3 content in ceramsite but does not influence the mass ratio of CaO to Fe_2O_3 (0.95). Based on the C3 constituent, BS is added to replace SS with ratios of 5%, 10%, 15%, and 20% to obtain the material constituents of the ceramsites with ternary components. As the BS replacement ratio increases, more CaO results in a higher total flux, with the ratio of CaO to Fe_2O_3 increasing from 0.95 to 2.13. The dry raw materials were subjected to a pellet mill, followed by the addition of water until complete pelletization was achieved. The water-to-solid mass ratio (*w/s*) for different groups is listed in Table 2. The obtained wet pellets were left in the ambient environment for 24 h and then dried at 105 °C until a constant weight was achieved. Afterward, they were placed in a muffle furnace to prepare the sintered ceramsite.

The thermal behaviors of the raw materials are shown in Fig. 3a–c. The total weight losses of SS, FA, and BS between 25 °C and 1000 °C are 36.2%, 7.5%, and 37.5%, respectively. In contrast, SS exhibits the most complex weight loss process among the raw materials. The weight loss of SS can be subdivided into three stages, as evidenced by the TG and DTG curves. Between 25 and 200 °C, the weight loss is primarily attributed to the removal of free and absorbed water. Double endothermic peaks between 200 and 600 °C are attributed to the combustion of organic matter[32]. A further weight loss period is observed between 600 and 800 °C, attributable to the decomposition of $CaCO_3$. The weight changes of FA between 25 and 200 °C and 600 and 800 °C are similar to those of SS, which are primarily attributable to the evaporation of free and absorbed water and the decomposition of $CaCO_3$, respectively. Beyond 800 °C, a continuous weight loss for SS and FA may be associated with Fe_2O_3 and sulfate decomposition[15,33,34]. The decomposition of $CaCO_3$ exerts a predominant influence on the weight loss of BS at temperatures ranging from 600 to 800 °C. At the same time, the endothermic peak is shifted to a higher temperature in comparison with that of SS and FA, which may be because the presence of Fe_2O_3 and SiO_2 has a promoting effect on the decomposition of $CaCO_3$[35].

Thermal behavior between 25 and 1300 °C is conducted on the raw ceramsite of C1, C3, and C7. As presented in Fig. 3d–f, due to the predominant content of SS, the TG and DTG curves of these mixtures are analogous to those of SS between 25 °C and 1000 °C, and the relative proportions of

Table 2. Material constituents and main chemical composition of ceramsites.

Ceramsite notation	SS:FA:BS	SiO_2 (%)	Al_2O_3 (%)	CaO (%)	Fe_2O_3 (%)	Total flux (%)	CaO/Fe_2O_3	*w/s*
C1	80%:20%:0%	36.7	16.4	15.2	16.0	46.9	0.95	0.63
C2	85%:15%:0%	36.0	15.5	15.7	16.5	48.4	0.95	0.61
C3	90%:10%:0%	35.3	14.6	16.2	17.0	50.0	0.95	0.61
C4	85%:10%:5%	33.8	14.1	19.4	16.2	52.1	1.20	0.56
C5	80%:10%:10%	32.3	13.5	22.7	15.3	54.2	1.48	0.58
C6	75%:10%:15%	30.8	12.9	26.0	14.5	53.6	1.79	0.50
C7	70%:10%:20%	29.3	12.3	29.2	13.7	58.3	2.13	0.50

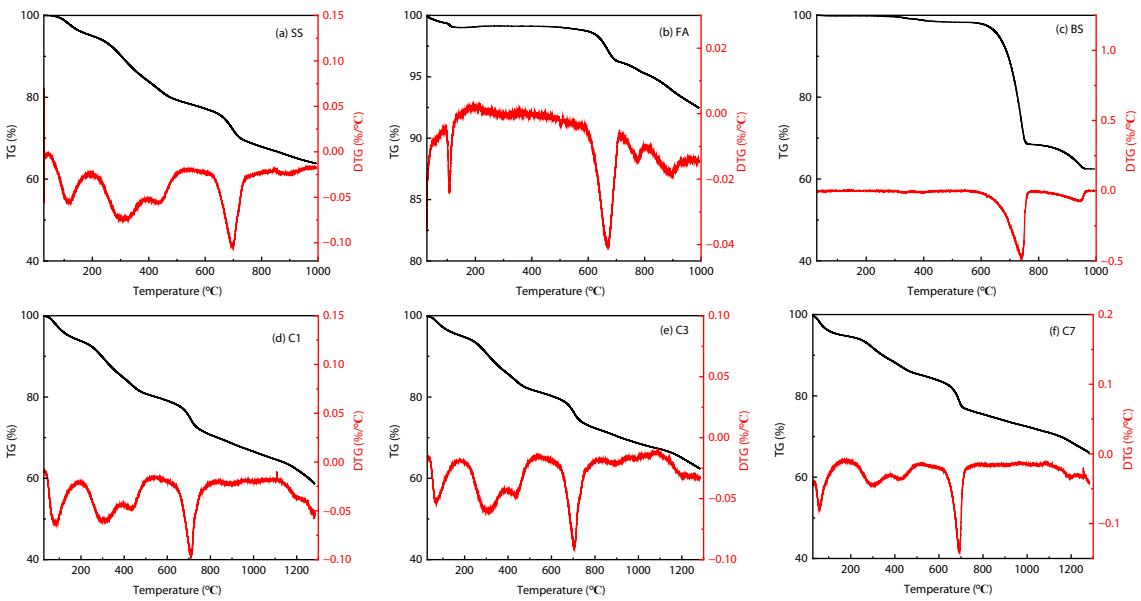

Fig. 3. Thermal behaviors of raw materials and raw ceramsites: (a) SS, (b) FA, (c) BS, (d) C1 ceramsite, (e) C3 ceramsite, and (f) C7 ceramsite.

the raw materials are found to have no significant influence on the thermal behaviors of the compounds. The endothermic peaks in the DTG curves, which appear at temperatures higher than 1000 °C, are indicative of the formation of the liquid phase[36]. It is suggested that the sintering temperature for the sludge ceramsite typically varies from 1000 °C to 1200 °C[37]. In terms of the $CaO\text{-}SiO_2\text{-}Al_2O_3$ system, a sintering temperature around 1150 °C is satisfactory for the formation of anorthite[14]. The study conducted by Liu et al.[21] indicates that ceramsite with diopside as the target phase can achieve high strength at temperatures between 1150 °C and 1160 °C. Accordingly, the sintering temperature of 1155 °C is set to form anorthite as the control phase and to investigate the influence of chemical composition on the phase transformation in different ceramsites. The sintering process can be summarized as follows: i) the ceramsite body was heated from ambient temperature to 300 °C over a period of 155 min and then maintained at this temperature for 10 min; ii) the temperature was increased to 1155 °C over a duration of 280 min; iii) the ceramsite was sintered at 1155 °C for 25 min; iv) a cooling process was initiated, during which the temperature was first reduced to 1000 °C over 45 min and then to room temperature at a rate of 2.8 °C min^{-1}.

2.3. Test methods

The ultimate load of a single porous ceramsite was tested using a compression tester, and the compressive strength was calculated by Equation (1), which has been widely used in previous studies[5,9,15,16]. The dimensions of the ceramsite were measured with a vernier caliper. Thirty particles were tested for each ceramsite.

$$F = 2.8P/\pi X^2 \quad (1)$$

where, F is the particle compressive strength of ceramsite, MPa; P is the ultimate load under compressive loading, N; X is the distance between two contact points of a porous ceramsite, mm.

The dried ceramsites were soaked in water for 24 h and then wiped with a wet towel. Water absorption was calculated as the difference in weight between water-saturated and dried ceramsites. The volume of the water-saturated sample was determined using an electronic hydrostatic balance, and the apparent density of the ceramsite was calculated as the dry mass divided by the volume.

The shrinkage of the ceramsite before and after sintering was evaluated using image processing. As shown in Fig. 4, after obtaining images of the ceramsite before and after sintering, the ceramsite particles were first highlighted. Then the area, perimeter, and Feret diameter were measured using an image analysis software. The roundness, as a shape factor, was calculated using Equation (2).

$$\text{Roundness} = (\text{Perimeter}^2)/(4 \times \pi \times \text{Area}) \quad (2)$$

The sintered ceramsites are crushed and ground to prepare powder samples with particle sizes smaller than 75 μm for thermal behavior and mineral constituent tests. The thermogravimetric (TG) analysis of raw materials and green ceramsite was conducted using a simultaneous thermal analyzer (SDT650) with a heating rate of 10 °C min^{-1} in the N_2 atmosphere. The test temperature ranges are 25–1000 °C and 25–1400 °C, respectively. The main mineral constituents of raw materials and sintered ceramsite were analyzed by an X-ray diffraction (XRD) analyzer. The XRD test was performed using an XRD diffractometer (Bruker D8-Advance, Cu Kα) with a scanning range of 5°–70°, a scanning rate of 10° min^{-1}, and a step length of 0.02°. Using the fragment samples, the microstructure of the sintered ceramsite was observed by scanning electron microscopy (SEM, Zeiss Sigma 300), and the element composition of the crystalline phases was analyzed by energy dispersive X-ray spectroscopy (EDS).

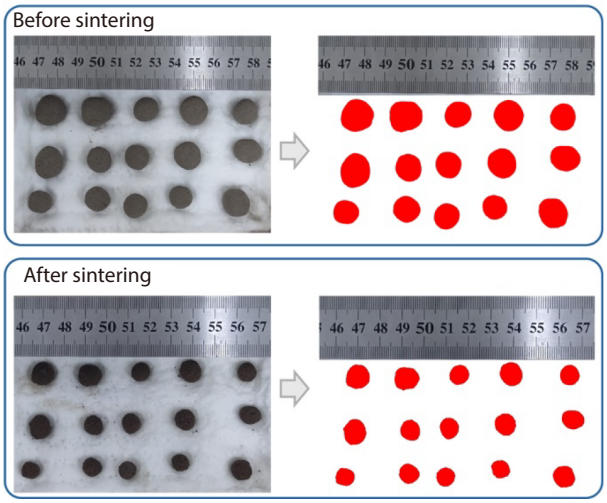

Fig. 4. Morphology analysis of the ceramsite before and after sintering.

The leaching of heavy metals is generally of concern for the ceramsite prepared from industrial solid waste. The leaching tests for heavy metals, such as Cr, Cu, Zn, Pb, and Hg, were conducted with the sulphuric acid & nitric acid method specified in the standard HJ/T 299-2007. The concentrations of Cr, Cu, Zn, and Pb in the leaching solution were detected using an inductively coupled plasma mass spectrometry (ICP-MS NexION 1000G), and the concentration of Hg was determined using an atomic fluorescence spectrometry (AFS-933).

3. Results and discussion

3.1. Macroscopic morphology

The sintering process is accompanied by a series of reactions, including mineral decomposition and phase transformations. These phenomena induce alterations in the mass and appearance of ceramsite. As shown in Fig. 5a–g, the ceramsites are effectively fabricated from the designed material constituents at 1155 °C. During the sintering process, the ceramsites preserve predominantly spherical morphologies. As illustrated in Fig. 5h, the influence of varied material constituents on ceramsite mass loss is negligible, yet a significant effect on ceramsite particle size is observed. In comparison with C3 ceramsite with 10% FA, C2 ceramsite with 15% FA exhibits a higher degree of area loss. However, as the FA content increases from 15% to 20%, the area loss decreases. With the content of FA fixed at 10%, replacing BS with SS induces signifi-

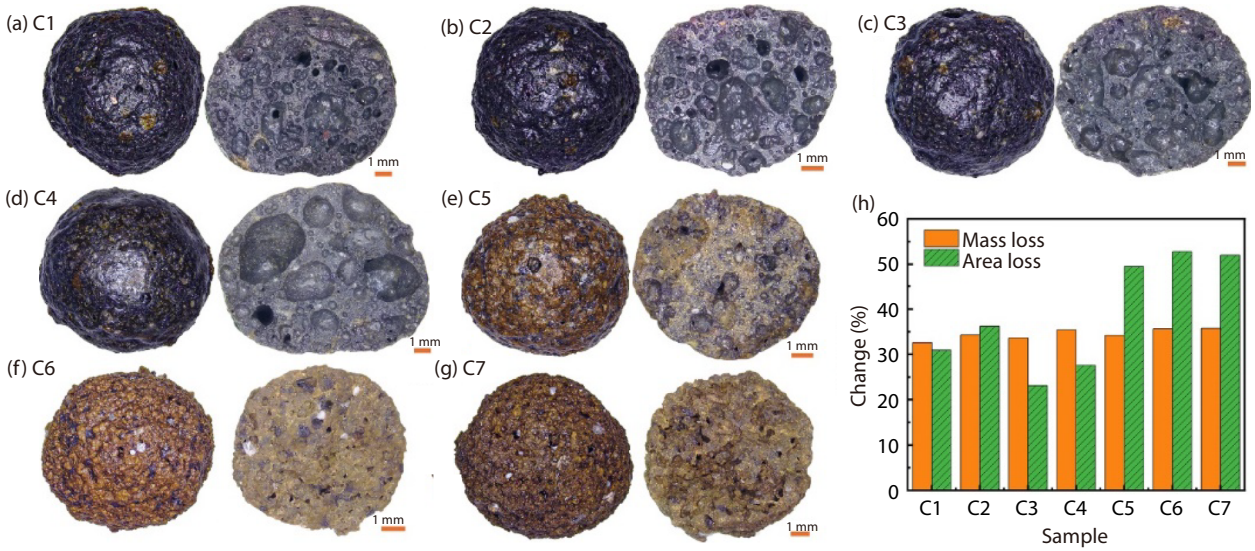

Fig. 5. Mass and shape changes of sintered ceramsites.

cant shrinkage, particularly at replacement ratios greater than 10%. The shrinking trend is strongly correlated with the pore structure observed in the cross-sections of ceramsites. The pores in C3, which exhibit a moderate size, are uniformly distributed on the cross-section of ceramsite. However, with an increase in FA content, pore size tends to decrease, resulting in a denser structure, and the pores exhibit a non-uniform distribution. A 5% BS content results in a significant increase in the pore size, but when the BS content exceeds 10%, the cross-section of ceramsite becomes densified with a limited number of pores. At a 20% BS content, the ceramsite surface becomes irregular with visible open pores. In addition, a BS content above 5% results in a shift in the color of sintered ceramsites from black to brown, which can be attributed to the chemical states of Fe_xO_y.

3.2. Physical-mechanical properties

The physical-mechanical properties of the sintered ceramsites are outlined in Fig. 6. The relationships between load and displacement during the compression test for ceramsite particles are plotted in Fig. 6a. It can be seen that all the prepared ceramsites exhibit brittle characteristics and similar stiffnesses. Fig. 6b illustrates the particle compressive strength, calculated from the ultimate load. The particle compressive strength of C3 ceramsite containing 10% FA is 7.13 MPa, and the compressive strength of the particles undergoes a decline as the FA content increases. Based on C3 ceramsite, replacing SS with 10% and 15% BS significantly improves the compressive strength of the ceramsite. The most effective replacement ratio is 15%, which results in a 141.5% increase in compressive strength compared to C3. However, an excessive replacement ratio (i.e., 20%) has a detrimental effect on the particle compressive strength.

Fig. 6c shows the apparent density of ceramsites with different material constituents. C3 ceramsite has the lowest apparent density of 1280 kg m^{-3}. Increasing the content of either FA or BS increases apparent density, with the effect of the latter being more pronounced. At a BS content of 15%, the apparent density reaches a maximum of 2196 kg m^{-3}. It is noteworthy that the influences of FA and BS on the apparent density are consistent with those on the size changes of ceramsites in Fig. 5h, thereby demonstrating the densification effect of different material constituents. However, the compressive strength is not totally decided by the compactness of ceramsite. C6 ceramsite has the highest specific strength of 7.8×10^{-3} MPa m^3 kg^{-1}, which may be attributed to the formation of high-strength phases with the optimum combination of 75% SS, 10% FA, and 15% BS. The water absorption of ceramsite is shown in Fig. 6d. Water absorption is a property associated with open porosity, which is affected by the stability of the liquid phase formed on the surface layer. As shown in Figs. 5 and 6, the surface state of ceramsite is closely related to its water absorption capacity. For C1–C5 ceramsites, a compact surface results in low water absorption. When the BS content exceeds 10%, the ceramsite surface becomes rougher due to the formation of more open pores, leading to a significant increase in water absorption.

3.3. Mineral constituents

The phase transformation of ceramsite with different material constituents is analyzed based on the XRD patterns shown in Fig. 7. As demonstrated in Fig. 7a, the crystal phases of ceramsites prepared from SS and FA comprise quartz, anorthite, hematite, augite, diopside, hedenbergite, cristobalite, magnetite, and fluorapatite. In the binary system of SS and FA, quartz, anorthite, and hematite have relatively intense diffraction peaks, which are responsible for the compressive strength of the ceramsite[19,38]. Additionally, the presence of magnetite in the ceramsites with SS and FA may be the primary reason for their black appearance.

As illustrated in Fig. 7b, the addition of BS has no influence on the mineral types of the sintered ceramsite but significantly changes the yield of different crystalline phases. It is clearly seen in Fig. 7c that when the addition of brine sludge exceeds 5%, the diffraction intensities of the characteristic quartz and hematite peaks decrease significantly. In contrast, the diffraction peak intensities at 29.9° and 35.1° are

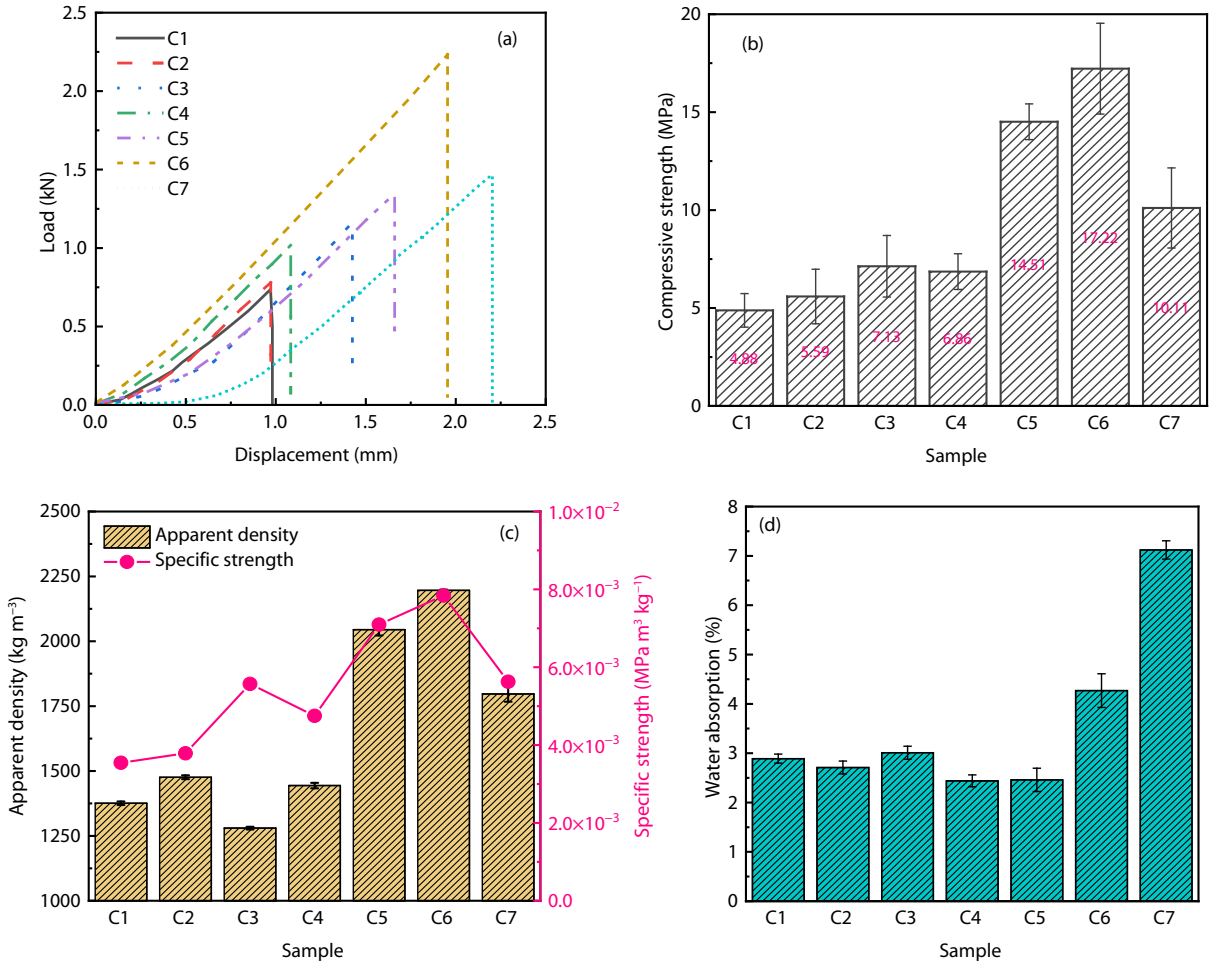

Fig. 6. Mechanical and physical properties of the sintered ceramsite: (a) load-displacement curves, (b) particle compressive strength, (c) apparent density and specific strength, and (d) water absorption.

enhanced, indicating an increase in the yield of augite, diopside, and hedenbergite. As shown in Fig. 7d, the diffraction peak intensities of augite, diopside, and hedenbergite in C6 are about 9 times those of C3. These results suggest that the addition of brine sludge promotes the dissolution of quartz while providing sufficient CaO to transform hematite into iron-containing crystalline phases such as augite, diopside, and hedenbergite. In addition, when the brine sludge content exceeds 15%, CaO exceeds the demand of the solid-phase reaction, resulting in no further increase in the yields of augite, diopside, and hedenbergite.

3.4. Chemical bonds

As shown in Fig. 8, the FTIR spectra provide further insight into the phase transformation behavior of the ceramsite during sintering. The chemical bonds are analyzed in accordance with the preceding studies[24,39–41]. The band observed at approximately 1040 cm^{-1} is indicative of the stretching vibration of Si–O bonds in amorphous silicon dioxide. The vibrations of Si–O–Al at 530 cm^{-1}, 757 cm^{-1}, and 936 cm^{-1} indicate the formation of aluminosilicate. The principal distinctions between the FTIR of different ceramsites become evident within 500–700 cm^{-1}, where C3 ceramsite exhibits a broad absorption band. However, an increase in the BS content splits the broad band into three peaks. The broader band indicates higher structural disorder, mostly due to the vitreous phase[23]. The peak at 566 cm^{-1} is characteristic of Fe–O vibration, and the intensifying peak at 680 cm^{-1} is attributed to the stretching and deformation vibrations of Si–O–Fe in diopside[23,24,41,42]. Notably, diopside can form a complete solid solution series with hedenbergite and augite. This further verifies that Fe_2O_3 participates in the solid-phase reactions to form crystalline phases.

3.5. Microstructure

As shown in Fig. 9, the microstructures of the ceramsites are observed at different magnifications. It is evident that C1 and C3 ceramsites, which contain differing FA content, possess a high number of pores formed from the gasification of the decomposable components. The microstructural images in Fig. 9b, c, e, and f illustrate that the pore walls of both C1 and C3 ceramsites are also characterized by porous structures, formed through particle packing. However, in the case of C3 ceramsite, the particles are bonded more tightly by a more vitreous phase. This is beneficial for the strength of the ceramsite. The addition of BS significantly influences the microstructure. As shown in Fig. 9g–l, C6 and C7 ceramsites, in comparison to C1 and C3 ceramsites, have fewer internal pores and exhibit denser pore walls comprising vitreous phases. This suggests that incorporating BS enhances the liquid phase, lead-

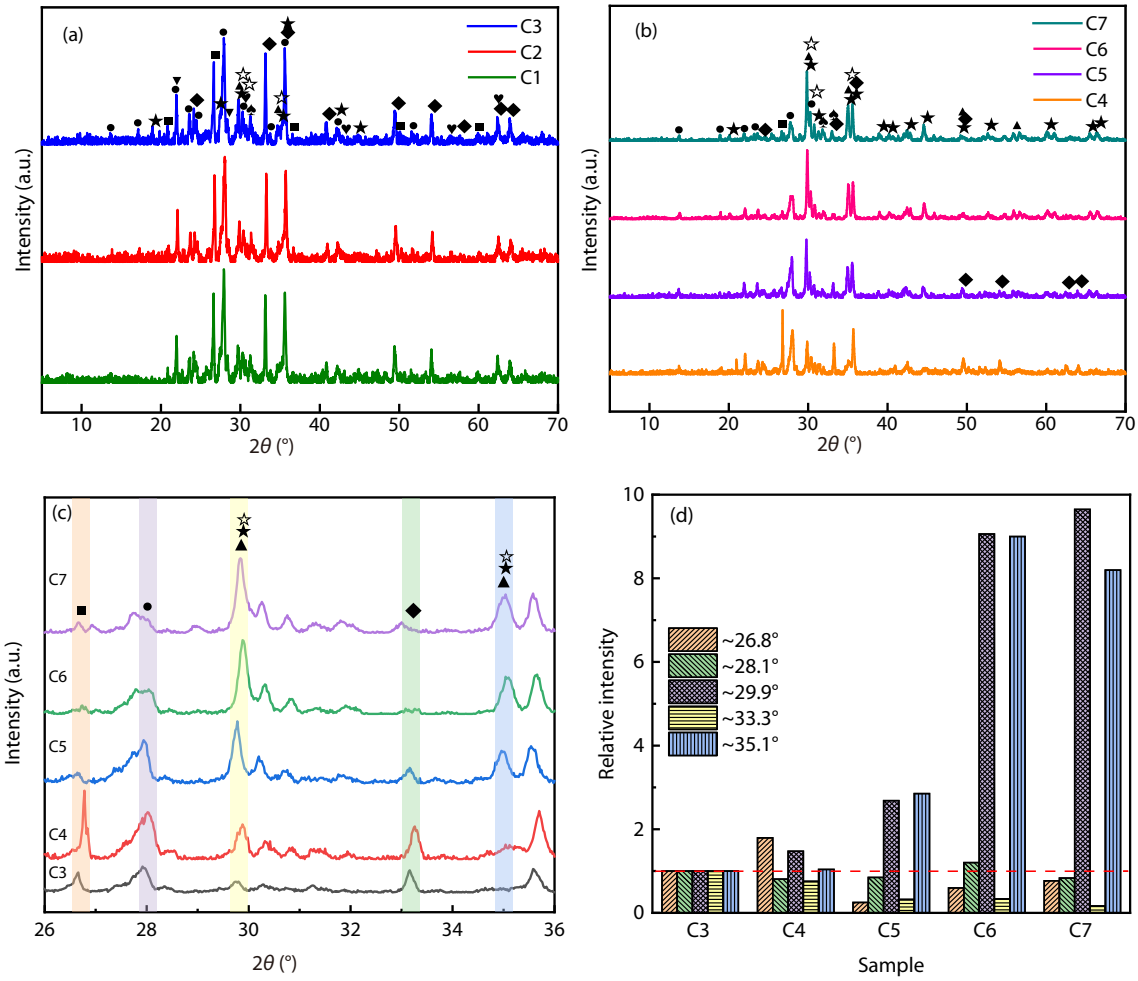

Fig. 7. XRD patterns of the sintered ceramsite: ■-Quartz (SiO_2), ●-Anorthite ($CaAl_2Si_2O_8$), ◆-Hematite (Fe_2O_3), ★-Augite ($Ca(Mg,Fe,Al)(Si,Al)_2O_6$), ☆-Diopside ($CaMgSi_2O_6$), ▲-Hedenbergite ($CaFeSi_2O_6$), ▼-Cristobalite, ♥-Magnetite (Fe_3O_4), ♠-Fluorapatite ($Ca_5(PO_4)_3F$).

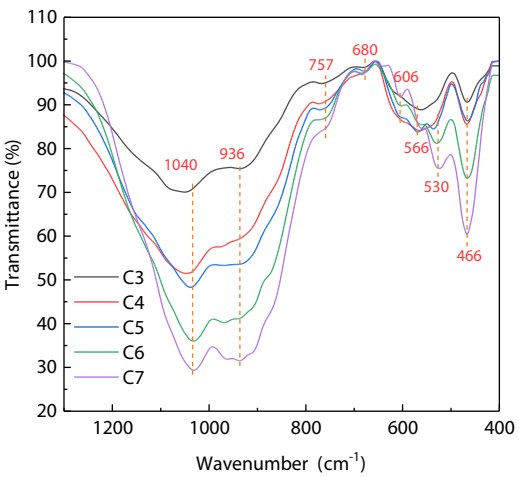

Fig. 8. FTIR spectra of the sintered ceramsite.

ing to pore filling and structural densification. Furthermore, the presence of fibrous crystals in C6 and C7 ceramsites, which are not observed in C1 and C3 ceramsites, suggests that these crystals may enhance the strength of the ceramsite matrix through their intertexture.

The elemental composition of the crystalline phases present in various ceramsites is determined using EDS. As shown in Table 3, the element composition of Al, Si, and Ca at Spots 1, 3, and 4 is close to that of anorthite ($CaAl_2Si_2O_8$), and P is rich in Spot 2, which belongs to fluorapatite as demonstrated by the XRD results. In comparison to the granular crystals in the C1 sample, the fibrous crystals in the C6 and C7 samples exhibit more complex element composition. Nevertheless, the fibrous crystals tend to contain more Ca and Fe, with slight decreases in Si and significant decreases in Al. In conjunction with the XRD analysis, it can be deduced that the fibrous crystals predominantly associate with augite, diopside, and hedenbergite, and the addition of BS promotes the transformation of anorthite into augite, diopside, and hedenbergite.

3.6. Heavy metal leaching

C3 and C6 ceramsites are selected for the heavy metal leaching tests. As presented in Table 4, all detected heavy metals are at much lower concentrations than the limit values specified in GB 5085.3-2007, with Zn, Pb, and Hg for both ceramsites being below the detection limits of inductively coupled plasma mass spectrometry and atomic fluorescence spectrometry. As pointed out by Xu et al.[6], high-temperature sintering at temperatures above 1000 °C significantly affects the solidification and stabilization of heavy metals. The solidification/stabilization mechanism of heavy metals is associated

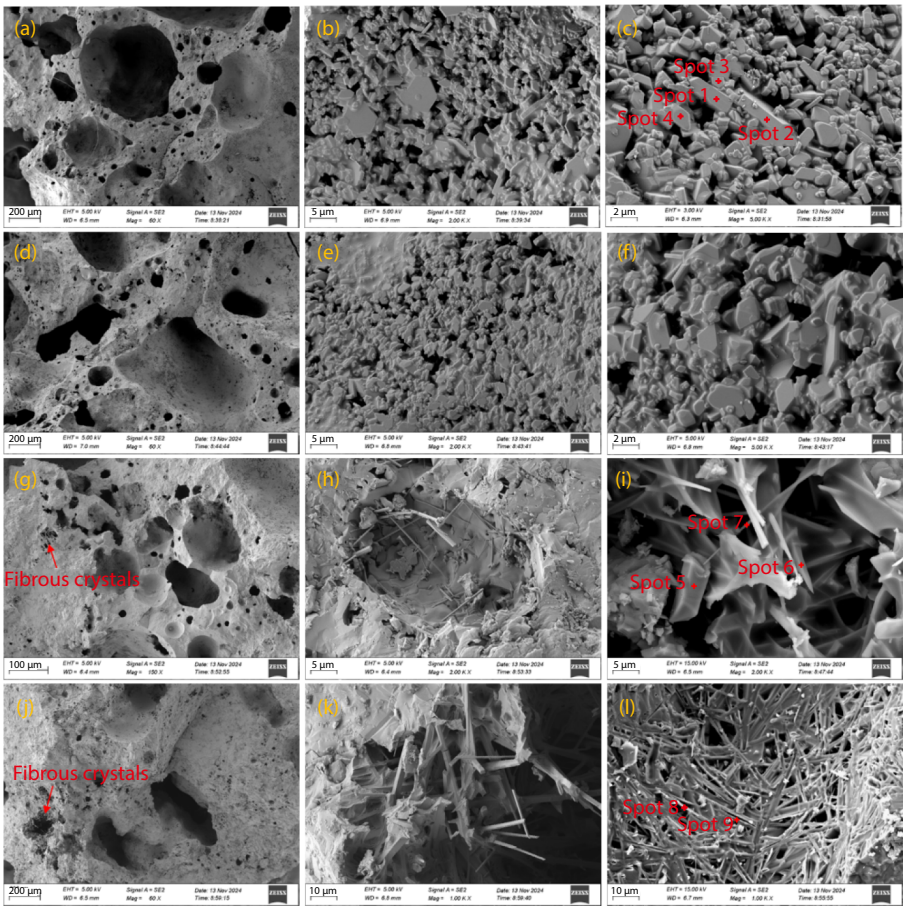

Fig. 9. SEM images of the sintered ceramsite: (a–c) C1, (d–f) C3, (g–i) C6, and (j–l) C7.

Table 3. Elemental composition of crystalline phases in different ceramsites determined by EDS (wt %).

Element	Spot 1	Spot 2	Spot 3	Spot 4	Spot 5	Spot 6	Spot 7	Spot 8	Spot 9
C	/	/	/	9.13	/	/	/	9.37	/
O	44.32	45.28	47.90	43.33	24.50	46.60	27.39	42.22	37.19
Na	1.53	/	1.57	1.15	0.32	1.13	1.03	2.03	4.23
Mg	/	1.96	/	/	3.67	3.98	0.53	2.48	/
Al	15.62	1.46	13.85	13.45	7.50	3.75	1.73	5.43	2.67
Si	24.09	2.84	23.35	19.83	20.98	17.27	15.35	14.55	17.98
P	/	17.16	/	/	/		6.16	/	4.42
K	/	/	/	/	/	0.57	2.12	/	/
Ca	11.05	28.24	9.45	9.66	21.58	13.38	36.99	20.02	22.17
Fe	3.38	1.69	3.88	3.46	21.45	13.32	8.70	3.89	7.27
S	/	1.36	/	/	/	/	/	/	/
Cu	/	/	/	/	/	/	/	/	4.08

Table 4. Leaching test results of heavy metals of ceramsite (μg L^{-1}).

Sample	Cu	Zn	Cr	Pb	Hg
C3 ceramsite	31.0	< 6.4	< 2.0	< 4.2	< 0.04
C6 ceramsite	31.6	< 6.4	27.8	< 4.2	< 0.04
Limits specified in GB 5085.3-2007	10^5	10^5	15000	5000	100

with vitreous and crystalline phases during sintering. The heavy metals are either wrapped by the vitreous phase in a highly compact manner or entrapped within the crystal structure by occupying vacancies or replacing other metal ions[24,43]. Besides, as claimed by Liu et al.[9], there exist appropriate contents of SiO_2 and Al_2O_3 for the solidification/stabilization of heavy metals, and the leaching content of Cr increases significantly when the Al_2O_3 content is less than

15%. The 15% BS replacement ratio for SS reduces the Al_2O_3 content from 14.6% to 12.3%, which may explain the stronger Cr leaching tendency in C6 ceramsite than in C3 ceramsite. On the other hand, C6 ceramsite has a higher water absorption than C3 ceramsite, which also facilitates the leaching of heavy metals.

3.7. Discussion

During sintering, the mass losses of SS and BS are similar and significantly higher than those of FA. In the binary system of SS and FA, the organic matter present in SS acts as the main gasifying agent and is the primary source of the formation of pores in the ceramsite. As the FA content increases from 10% to 20%, the gas yield from SS decreases, resulting in a reduction in the porosity of the ceramsite and an increase in its apparent density. However, due to the reduced flux content and the decreased amount of vitreous phase, the bonding between crystals weakens, leading to reduced strength.

Replacing SS with BS has little effect on gas yield, but increasing the calcium oxide (CaO) content facilitates the depolymerization of the silicate network[44,45], and the increase in flux content lowers the eutectic point, thereby promoting the melting of quartz and hematite, forming a large amount of low-viscosity liquid phase[36,46,47]. However, the lower viscosity of the liquid phase limits its ability to trap pores, causing them to merge into larger ones and allowing gas to escape[43]. In addition, the decomposition temperature of calcium carbonate ($CaCO_3$) is higher than that of the organic matter in SS. As the BS content increases, more gas is generated in the later stages of sintering, and the greater expansion force produced makes the gas more likely to penetrate the liquid phase and escape.

In terms of phase transformations, compared with binary ceramsite containing SS and FA, the introduction of BS changes the main crystalline phases from quartz, anorthite, and hematite to pyroxenes, such as augite, diopside, and hedenbergite. Due to the high valence and small ionic radius of Ca^{2+}, it can replace Si^{4+} in the silicate network, forming anorthite[20,44]. The chemical composition of pyroxene group minerals can be expressed by the general formula XYZ_2O_6 (X = Na^+, Ca^{2+}, Mn^{2+}, Fe^{2+}, Mg^{2+}, Li^+; Y = Mn^{2+}, Fe^{2+}, Mg^{2+}, Fe^{3+}, Al^{3+}, Cr^{3+}, Ti^{4+}; and Z = Si^{4+}, Al^{3+}). For the prepared ceramsite, reactions described by Equations (3) to (5) can produce Fe in different valence states[5,22]. When the Y site is completely substituted by Fe, the resulting mineral is hedenbergite. The formation of anorthite is prioritized over pyroxene minerals[16], assuming that CaO first combines with Al_2O_3 and SiO_2 to form anorthite, while the remaining CaO coordinates with Fe_2O_3 to form hedenbergite. The amount of CaO required for the formation of anorthite and hedenbergite is shown in Table 5. It can be seen that the addition of BS can compensate for the insufficient CaO content in binary ceramsite. When the BS content is 5%, Fe_2O_3 can be completely converted into hedenbergite. However, due to the presence of other ions such as Na^+, K^+, and Mg^{2+}, in addition to hedenbergite, Fe_2O_3 can actually also transform into augite and diopside, necessitating more CaO to participate in the solid-phase reaction. According to XRD analysis, a 15% addition of BS maximizes pyroxene formation, and a large number of fibrous pyroxene crystals interweave within the pores, enhancing the strength of the ceramsite. Accordingly, the mass ratio of $CaO/(Al_2O_3+Fe_2O_3)$ may be an effective parameter for the material design of ternary ceramsite composed of SS, FA, and BS.

$$3Fe_2O_3 + CO \rightarrow 2Fe_3O_4 + CO_2 \quad (3)$$

$$Fe_3O_4 + CO \rightarrow 3FeO + CO_2 \quad (4)$$

$$6Fe_2O_3 \rightarrow 4Fe_3O_4 + O_2 \quad (5)$$

4. Conclusions

A multi-source solid waste-based ceramsite is formulated by incorporating sewage sludge (70%–90%), fly ash (10%–20%), and brine sludge (0%–20%). With sewage sludge as the predominant constituent, the influence of fly ash and brine sludge replacement on the properties, phase transformation, and microstructure of the sintered ceramsite is investigated. Based on the experimental results, the following conclusions are drawn.

1) For the binary ceramsite composed of sewage sludge and fly ash, the ceramsite with 10% fly ash content has the highest strength and the lowest apparent density. Based on the optimized binary ceramsite, the addition of brine sludge increases the apparent density and significantly enhances the strength of ceramsite. When 15% of sewage sludge is replaced with brine sludge, the ceramsite has the maximum strength, and the specific strength increases from 5.6×10^{-3} to 7.8×10^{-3} MPa m^3 kg^{-1}.

2) The mineral composition of sintered ceramsite is mainly quartz, anorthite, hematite, and pyroxene. The addi-

Table 5. Comparison of theoretical and actual CaO amounts in ceramsites.

Sample	$CaAl_2Si_2O_8$		$CaFeSi_2O_6$		Theoretical CaO (%)	Actual CaO (%)	$CaO/(Al_2O_3+Fe_2O_3)$
	Al_2O_3 (%)	CaO (%)	Fe_2O_3 (%)	CaO (%)			
C1	16.4	9.0	16.0	11.2	20.2	15.2	0.47
C2	15.5	8.5	16.5	11.6	20.1	15.7	0.49
C3	14.6	8.0	17.0	11.9	19.9	16.2	0.51
C4	14.1	7.8	16.2	11.3	19.1	19.4	0.64
C5	13.5	7.4	15.3	10.7	18.1	22.7	0.79
C6	12.9	7.1	14.5	10.2	17.2	26.0	0.95
C7	12.3	6.8	13.7	9.6	16.4	29.2	1.12

tion of brine sludge promotes the melting of quartz and hematite, leading to increased pyroxene formation. Adding 15% brine sludge can convert almost all of the hematite into pyroxene. In addition, the ceramsites with varied mineral compositions have relatively low risks of heavy metal leaching.

3) The compressive strength of ceramsite is correlated with the formation of fibrous pyroxene. It is feasible to prepare high-strength, lightweight ceramsite with pyroxene as the target phase. At the same time, the mass ratio of $CaO/(Al_2O_3+Fe_2O_3)$ can serve as a key parameter in designing the ceramsite with multi-source solid waste.

Acknowledgements

This work was supported by the Natural Science Foundation of Henan Province (232300420291) and the National Natural Science Foundation of China (52304420).

Data availability

All data needed to support the conclusions in the paper are presented in the manuscript. Additional data related to this paper may be requested from the corresponding author upon request.

Declaration of competing interest

The authors declare the following financial interests/personal relationships which may be considered as potential competing interests: Feiyu Wang and Yang Liu are employed by China Construction Eighth Engineering Division Co., LTD (North China).

Author contribution statement

Gelong Xu: Conceptualization, Methodology, Writing – original draft. **Jiaqi Zhang:** Formal analysis, Investigation, Writing – original draft. **Jiwei Cai:** Methodology. **Feiyu Wang:** Resources. **Yang Liu:** Resources. **Xinyuan Feng:** Investigation. **Yaguang Wang:** Supervision. **Zixuan Du:** Investigation. **Qing Tian:** Formal analysis, Writing – review & editing.

Use of AI statement

None

References

[1] Qiao, C., Gu, D., Lu, G., et al. Research progress on sludge resource utilization in urban domestic sewage treatment plants. *Industrial Water Treatment*, **2024**, 45(7): 1–10. https://doi.org/10.19965/j.cnki.iwt.2024-0671.

[2] Kominko, H., Gorazda, K., Wzorek, Z. Sewage sludge: A review of its risks and circular raw material potential. *Journal of Water Process Engineering*, **2024**, 63: 105522. https://doi.org/10.1016/j.jwpe.2024.105522.

[3] Zhou, H., Wei, L., Wang, D., et al. Environmental impacts and optimizing strategies of municipal sludge treatment and disposal routes in China based on life cycle analysis. *Environment International*, **2022**, 166: 107378. https://doi.org/10.1016/j.envint.2022.107378.

[4] Fytili, D., Zabaniotou, A. Utilization of sewage sludge in EU application of old and new methods: A review. *Renewable and Sustainable Energy Reviews*, **2008**, 12(1): 116–140. https://doi.org/10.1016/j.rser.2006.05.014.

[5] Li, X., He, C., Lv, Y., et al. Utilization of municipal sewage sludge and waste glass powder in production of lightweight aggregates. *Construction and Building Materials*, **2020**, 256: 119413. https://doi.org/10.1016/j.conbuildmat.2020.119413.

[6] Xu, G. R., Zou, J. L., Li, G. B. Stabilization of heavy metals in sludge ceramsite. *Water Research*, **2010**, 44(9): 2930–2938. https://doi.org/10.1016/j.watres.2010.02.014.

[7] He, B., Wang, G. Is ceramsite the last straw for sewage sludge disposal: A review of sewage sludge disposal by producing ceramsite in China. *Water Science and Technology*, **2019**, 80(1): 1–10. https://doi.org/10.2166/wst.2019.223.

[8] Tsai, C. C., Wang, K. S., Chiou, I. J. Effect of SiO_2–Al_2O_3–flux ratio change on the bloating characteristics of lightweight aggregate material produced from recycled sewage sludge. *Journal of Hazardous Materials*, **2006**, 134(1/2/3): 87–93. https://doi.org/10.1016/j.jhazmat.2005.10.035.

[9] Liu, M., Liu, X., Wang, W., et al. Effect of SiO_2 and Al_2O_3 on characteristics of lightweight aggregate made from sewage sludge and river sediment. *Ceramics International*, **2018**, 44(4): 4313–4319. https://doi.org/10.1016/j.ceramint.2017.12.022.

[10] Wu, G., Yazhenskikh, E., Hack, K., et al. Viscosity model for oxide melts relevant to fuel slags. Part 2: The system SiO_2–Al_2O_3–CaO–MgO–Na_2O–K_2O. *Fuel Processing Technology*, **2015**, 138: 520–533. https://doi.org/10.1016/j.fuproc.2015.06.031.

[11] Kwon, S. Y., Hill, R. J., Jung, I. H. Multi-ion diffusion model and application to solid dissolution in CaO–Al_2O_3–SiO_2melts. *Journal of the American Ceramic Society*, **2024**, 107(3): 1835–1847. https://doi.org/10.1111/jace.19405.

[12] Xu, G., Zou, J., Li, G. Ceramsite made with water and wastewater sludge and its characteristics affected by SiO_2 and Al_2O_3. *Environmental Science & Technology*, **2008**, 42(19): 7417–7423. https://doi.org/10.1021/es801446h.

[13] Cheng, G., Li, Q., Su, Z., et al. Preparation, optimization, and application of sustainable ceramsite substrate from coal fly ash/waterworks sludge/oyster shell for phosphorus immobilization in constructed wetlands. *Journal of Cleaner Production*, **2018**, 175: 572–581. https://doi.org/10.1016/j.jclepro.2017.12.102.

[14] Jia, G., Wang, Y., Yang, F., et al. Preparation of CFB fly ash/sewage sludge ceramsite and the morphological transformation and release properties of sulfur. *Construction and Building Materials*, **2023**, 373: 130864. https://doi.org/10.1016/j.conbuildmat.2023.130864.

[15] Zhang, W., Zhao, Q., Peng, S., et al. Preparation and property evolution mechanism of high sludge-content ceramsite with blast furnace slag and red mud. *Journal of Water Process Engineering*, **2025**, 71: 107284. https://doi.org/10.1016/j.jwpe.2025.107284.

[16] Zhao, H., Wang, X., Zhang, X., et al. Preparation of high-strength ceramsite *via* co-sintering of shield tunnel muck and steel slag: Correlation investigation on phase composition and particle strength. *Construction and Building Materials*, **2024**, 439: 137413. https://doi.org/10.1016/j.conbuildmat.2024.137413.

[17] Wang, L. S., Wang, Y. X., Sun, W., et al. Preparation of lightweight and high-strength ceramsite from highly doped coal fly ash. *Transactions of Nonferrous Metals Society of China*, **2023**, 33(12): 3885–3898. https://doi.org/10.1016/S1003-6326(23)66378-2.

[18] Wang, J., Ma, Y., Li, J., et al. Preparation of egg-structured ceramsites from molybdenum tailings with improved properties. *Case Studies in Construction Materials*, **2024**, 20: e03303. https://doi.org/10.1016/j.cscm.2024.e03303.

[19] Long, Y., Pu, K., Yang, Y., et al. Preparation of High-strength ceramsite from municipal solid waste incineration fly ash and

clay based on CaO-SiO_2-Al_2O_3 system. *Construction and Building Materials*, **2023**, 368: 130492. https://doi.org/10.1016/j.conbuildmat.2023.130492.

[20] Wang, X., Qin, Y., Okeke, I., et al. Revealing the intrinsic sintering mechanism of high-strength ceramsite from CFB fly ash: Focus on the role of CaO. *Ceramics International*, **2024**, 50(13): 24281–24292. https://doi.org/10.1016/j.ceramint.2024.04.158.

[21] Liu, Y., Wan, W., Yang, F., et al. Performance of glass-ceramic-based lightweight aggregates manufactured from waste glass and muck. *Ceramics International*, **2022**, 48(16): 23468–23480. https://doi.org/10.1016/j.ceramint.2022.04.342.

[22] Zou, J. L., Xu, G. R., Li, G. B. Ceramsite obtained from water and wastewater sludge and its characteristics affected by Fe_2O_3, CaO, and MgO. *Journal of Hazardous Materials*, **2009**, 165(1/2/3): 995–1001. https://doi.org/10.1016/j.jhazmat.2008.10.113.

[23] Li, X., Wang, P., Guo, Z., et al. Effect of Fe^{2+}/Fe^{3+} on high-strength ceramsite prepared by sintering geopolymers using iron ore tailings. *Ceramics International*, **2022**, 48(4): 5681–5688. https://doi.org/10.1016/j.ceramint.2021.11.113.

[24] Zhang, C., Ren, Z., Wang, L., et al. The synergistic sintering of ultra-lightweight ceramsite from molybdenum ore tailings, iron ore tailings and waste glass powders: Properties and formation mechanism. *Construction and Building Materials*, **2024**, 452: 138852. https://doi.org/10.1016/j.conbuildmat.2024.138852.

[25] Chen, H., Song, M., Sui, Y., et al. Characterization and synergistic hydration mechanism of a low-carbon binder from MSWI fly ash and chlor-alkali salt mud. *Environmental Research*, **2026**, 300: 124401. https://doi.org/10.1016/j.envres.2026.124401.

[26] Garg, M., Pundir, A. Utilization of brine sludge in nonstructural building components: A sustainable approach. *Journal of Waste Management*, **2014**, 2014: 389316. https://doi.org/10.1155/2014/389316.

[27] Chepkonga, B. J., Koech, L., Makomere, R. S., et al. Machine learning and response surface methodology forecasting comparison for improved spray dry scrubber performance with brine sludge-derived sorbent. *Digital Chemical Engineering*, **2025**, 14: 100214. https://doi.org/10.1016/j.dche.2024.100214.

[28] Assaggaf, R. A., Alhajji, L., Siddique, S., et al. Accelerated carbonation curing of building mortars incorporating volcanic ash and brine sludge. *Construction and Building Materials*, **2024**, 438: 137267. https://doi.org/10.1016/j.conbuildmat.2024.137267.

[29] De Carvalho Izidoro, J., Fungaro, D. A., Viviani, L. C., et al. Brine sludge waste from a Chlor-alkali industry: Characterization and its application for non-structural and structural construction materials. *Journal of Applied Materials and Technology*, **2021**, 3(1): 1–7. https://doi.org/10.31258/jamt.3.1.1-7.

[30] Yan, X., Zhang, X., Wu, X. Research progress on comprehensive utilization of brine sludge resources. *Environmental Protection Science*, **2023**, 49: 85–92. https://doi.org/10.16803/j.cnki.issn.1004-6216.202305044.

[31] Li, X., Zeng, H., Sun, N., et al. Preparation of lightweight ceramsite by stone coal leaching slag, feldspar, and pore-forming reagents. *Construction and Building Materials*, **2023**, 370: 130642. https://doi.org/10.1016/j.conbuildmat.2023.130642.

[32] Franus, M., Madej, J., Panek, R., et al. Effect of microwave radiation temperature and content of different solid waste on the microstructure and physicomechanical properties of lightweight aggregates. *Ceramics International*, **2024**, 50(2): 2871–2886. https://doi.org/10.1016/j.ceramint.2023.11.021.

[33] Luo, Y., Wang, J., Wu, Y., et al. Substitution of quartz and clay with fly ash in the production of architectural ceramics: A mechanistic study. *Ceramics International*, **2021**, 47(9): 12514–12525. https://doi.org/10.1016/j.ceramint.2021.01.109.

[34] Liu, Z., Guo, R., Pan, T., et al. Preparation of ceramsite from low-silicon red mud (LSRM): Effects of Si–Al ratio and sintering temperature. *Ceramics International*, **2023**, 49(21): 34191–34204. https://doi.org/10.1016/j.ceramint.2023.08.131.

[35] Lu, H., Li, C. X., Mao, W. W., et al. Laboratory study of $CaCO_3$ decomposition, influence of BOF converter slag. *Metallurgical Research & Technology*, **2017**, 114(1): 119. https://doi.org/10.1051/metal/2016070.

[36] Guo, P., Zhao, Z., Li, Y., et al. Co-utilization of iron ore tailings and coal fly ash for porous ceramsite preparation: Optimization, mechanism, and assessment. *Journal of Environmental Management*, **2023**, 348: 119273. https://doi.org/10.1016/j.jenvman.2023.119273.

[37] Wang, H., Xu, J., Liu, Y., et al. Preparation of ceramsite from municipal sludge and its application in water treatment: A review. *Journal of Environmental Management*, **2021**, 287: 112374. https://doi.org/10.1016/j.jenvman.2021.112374.

[38] Scribot, C., Maherzi, W., Benzerzour, M., et al. A laboratory-scale experimental investigation on the reuse of a modified red mud in ceramic materials production. *Construction and Building Materials*, **2018**, 163: 21–31. https://doi.org/10.1016/j.conbuildmat.2017.12.092.

[39] Pei, J., Pan, X., Qi, Y., et al. Preparation and characterization of ultra-lightweight ceramsite using non-expanded clay and waste sawdust. *Construction and Building Materials*, **2022**, 346: 128410. https://doi.org/10.1016/j.conbuildmat.2022.128410.

[40] Peng, C., Dai, G., Wang, Y., et al. Preparation of high-strength ceramsite from coal gangue and printing and dyeing sludge: Design strategy and modelling mechanism. *Ceramics International*, **2024**, 50(11): 19963–19970. https://doi.org/10.1016/j.ceramint.2024.03.122.

[41] Xiao, T., Wang, Y., Fan, X., et al. Preparation of eco-friendly and high-strength ceramsite by granite scraps, granite fine mud, and phosphogypsum: Response surface methodology optimization, environmental safety assessment. *Process Safety and Environmental Protection*, **2024**, 192: 960–972. https://doi.org/10.1016/j.psep.2024.10.085.

[42] Zhan, X., Zhang, D., Wang, J., et al. Preparation of lightweight ceramsite from municipal solid waste incineration ash and tuff: Constrained uniform mixture design, thermodynamic simulation and formation mechanism. *Construction and Building Materials*, **2024**, 456: 139315. https://doi.org/10.1016/j.conbuildmat.2024.139315.

[43] Pei, J., Pan, X., Qi, Y., et al. Preparation of ultra-lightweight ceramsite from red mud and immobilization of hazardous elements. *Journal of Environmental Chemical Engineering*, **2022**, 10(4): 108157. https://doi.org/10.1016/j.jece.2022.108157.

[44] Zhou, M., Ge, X., Wang, H., et al. Effect of the CaO content and decomposition of calcium-containing minerals on properties and microstructure of ceramic foams from fly ash. *Ceramics International*, **2017**, 43(12): 9451–9457. https://doi.org/10.1016/j.ceramint.2017.04.122.

[45] Liu, Q., Wang, W., Gao, M., et al. Effect of CaO/SiO_2 and Al_2O_3/SiO_2 mass ratios on structure and viscosity of mold flux for continuous casting high-Mn high-Al steel. *Steel Research International*, **2025**, 96(6): 2400740. https://doi.org/10.1002/srin.202400740.

[46] Xiong, X., Chen, H., Jiang, P., et al. Honeycombed pomegranate-like sludge ceramsite particles: Preparation with fly ash floating beads as the pore-forming template and performance optimization. *Construction and Building Materials*, **2024**, 453: 139017. https://doi.org/10.1016/j.conbuildmat.2024.139017.

[47] Ayati, B., Ferrándiz-Mas, V., Newport, D., et al. Use of clay in the manufacture of lightweight aggregate. *Construction and Building Materials*, **2018**, 162: 124–131. https://doi.org/10.1016/j.conbuildmat.2017.12.018.

Gelong Xu, an Associate Professor at the School of Civil Engineering and Architecture, Henan University, received his PhD degree from Wuhan University of Technology in 2020. He has published over 30 academic papers, with research interests including low-carbon cementitious materials, insulation materials, and the comprehensive utilization of solid waste.

Qing Tian is an Associate Professor at the School of Civil Engineering and Architecture, Henan University. He received a PhD degree from Central South University in 2017 and has since published more than 20 academic papers in leading domestic and international journals. His primary research focuses on high-performance cementitious materials and the comprehensive utilization of solid waste.